Chapter 3

Analysis of the laminar flamelet concept for non-premixed laminar flames. Application to the numerical simulation of a confined co-flow methane/air flame

Contents of this chapter are submitted to *Combustion and Flame* journal.

The goal of this paper is to investigate the application of the laminar flamelet concept to the multidimensional numerical simulation of non-premixed laminar flames. The performance of steady and unsteady flamelets is analysed. The deduction of the mathematical formulation of the flamelet modelling is exposed and some commonly used simplifications are examined. Different models for the scalar dissipation rate dependence on the mixture fraction variable are analysed. Moreover, different criteria to evaluate the Lagrangian type flamelet lifetime for unsteady flamelets are investigated. Inclusion of phenomena as differential diffusion with constant Lewis number for each species and radiation heat transfer are also studied. A confined co-flow axisymmetric non-premixed methane/air laminar flame experimentally investigated by [1], and numerically investigated by [2–4], has been used as a test case. Results obtained using the flamelet concept have been compared to data obtained from the full resolution of the complete transport equations using primitive variables. Finite volume techniques over staggered grids are used to discretize the governing equations. A parallel multiblock algorithm based on domain decomposition techniques running with loosely coupled computers has been used. To assess the quality of the numerical solutions

presented in this paper, a verification process based on the generalised Richardson extrapolation technique and on the Grid Convergence Index (GCI) has been applied.

3.1 Introduction

Fluid dynamics, heat and mass transfer phenomena involved in combustion systems is governed by continuity, momentum, energy and species transport equations, together with state equation. The considerable complex phenomena involved, often three-dimensional turbulent flames with radiatively participating media and large kinetic mechanisms, hardly allow the resolution of detailed models forcing the assumption of restrictive hypothesis in the development of computational capable models. The laminar flamelet concept assumption can contribute both in laminar and specially in turbulent flames to reduce this computational effort. Even though this concept is not new, its study and application has increased and improved during the last two decades [5, 6]. Turbulent combustion flames are the main interest and widespread application of the laminar flamelet concept, but its idea arises from the laminar combustion.

Assuming a one-dimensional behaviour of the combustion phenomena in the normal direction to the flame front, from energy and species transport equations and applying a coordinate transformation, flamelet equations can be derived. In these equations, temperature and species mass fractions are function of a conserved scalar known as mixture fraction (Z). In addition, a parameter called scalar dissipation rate (χ) totally represents the influence of the flow field on the flamelet structure.

Flamelet equations are solved in advance in a pre-processing task, modelling a scalar dissipation rate distribution and building the *flamelet libraries*. In CFD laminar flame simulations, species and temperature can be evaluated from the flamelet libraries. Only a transport equation for the mixture fraction needs to be solved during the simulation, being the scalar dissipation rate χ evaluated from the mixture fraction distribution. In this sense, the number of equations to be solved is dramatically reduced and the stiffness inherent to the combustion mechanisms is treated in the mentioned pre-processing task.

The flamelet approach can be considered as an extension of the "flame sheet" model which assumes infinitely fast chemical reactions, such that the reaction zone is an infinitely thin interface. The fast chemistry assumption fails whenever non-equilibrium effects such us extinction, re-ignition, lift-off and blow-out are important. Moreover, the assumption of fast chemistry for some intermediate species like CO and H_2 and NO_x formation results in an over-prediction of the mass fraction of these species since they are involved in slow reactions. Carbon monoxide (CO) oxidation to carbon dioxide (CO_2) is slow and formation times of thermal nitrogen oxide (NO_x) are even longer [7]. This suggests that non-equilibrium effects are important in modelling these flames. The flamelet approach relaxes the infinitely fast chemistry

assumption by introducing, in addition to the mixture fraction, the scalar dissipation rate as a parameter to describe the degree of departure from the equilibrium state [8]. Some other models have been successful in close-to-equilibrium flames (see review in [5]). Nevertheless, far-from-equilibrium effects such as flame extinction are typically present in many flames, and a methodology designed to incorporate these effects is not only desirable but necessary.

However, the *steady flamelet* approach still relies on the assumption that the time scales for chemical kinetics are much shorter than the time scales of convection and diffusion. Under this condition of widely separated time scales, the combustion chemistry reaches a quasi-steady state and immediately adjusts to local flow conditions. Some phenomena, e.g. radiation heat transfer or pollutant formation of NO_x, do not accomplish this requirement of separated time scales. These are slow processes compared to main chemical time scales and can have a characteristic time scale of the same order of magnitude of the convective or diffusive ones. In order to overcome the limitations that steady flamelets assumption introduce, *unsteady flamelets* can be taken into account.

Even though the common application of flamelet modelizations is the numerical simulation of turbulent flames, deep knowledge of the capabilities and limitations of the laminar flamelet approximation can be emphasised in the numerical simulation of laminar flames. Considering that the flamelet concept arises from a transformation of the basic mathematical formulation, a rigorous analysis can be performed comparing flamelet modelling simulations with reference solutions based on the full resolution of the transport equations. In the present work, a confined co-flow axisymmetric non-premixed methane/air laminar flame [1] numerically analysed in [2–4] is considered.

The deduction of the mathematical governing equations of the flamelet modelling is exposed and some commonly used simplifications are examined. Inclusion of phenomena, such as differential diffusion and radiation heat transfer, are also studied. A comparison of steady and unsteady flamelets is performed highlighting the main advantages and restrictions of each approach. Different models for the scalar dissipation rate dependence on the mixture fraction variable are analysed. For unsteady flamelets, different criteria to evaluate the Lagrangian type flamelet lifetime are investigated.

3.2 Flamelet model formulation and implementation

3.2.1 Conserved scalar approach. Mixture fraction

Diffusion flames constitute a specific class of combustion problems where fuel and oxidizer are not mixed before they enter into the combustion chamber. For these flames, mixing must bring reactants into the reaction zone fast enough for combustion

to proceed [7]. Thus, the proper description of the mixing process is a key aspect of non-premixed combustion.

In general, the structure of non-premixed flames can be described by means of a conserved scalar, which is chemically independent (non-reacting). This variable is the so-called mixture fraction (Z) [9, 10]. Z is a passive (or conserved) scalar that accounts for the level of mixing between the oxidizer and the fuel and changes because of diffusion and convection, but not reaction. It is generally convenient to scale Z in the range 0-1. A transport equation for the mixture fraction can be posed as follows [11]:

$$\frac{\partial(\rho Z)}{\partial t} + \nabla \cdot (\rho \vec{v} Z) = \nabla \cdot (\rho D_z \nabla Z) \tag{3.1}$$

In this equation ρ is the density and D_z is the diffusion coefficient of the mixture fraction equation. A Lewis number Le_z can be defined as $Le_z = \lambda/(\rho D_z c_p)$, where λ is the thermal conductivity and c_p the specific heat at constant pressure.

Main differences to previous formulations is the definition of a mixture fraction variable which is not directly related to any combination of the reactive scalars, but defined from a conservation equation with an arbitrary diffusion coefficient and appropriate boundary conditions [11]. This definition allows a general treatment in the deduction of the flamelet equations including phenomena as differential diffusion. Using this definition, flamelet equations with the mixture fraction as the independent coordinate can be derived without any assumptions about the Lewis numbers for chemical species [11].

3.2.2 Flamelet equations

A flame can be viewed as an ensemble of thin locally one-dimensional structures embedded within the flow field. Each element of the flame front can then be viewed as a small laminar flame also called *flamelet* [7, 10]. Physically, the flame structure is considered locally one-dimensional and only depends on time and the coordinate normal to the flame front.

A coordinate system attached to the surface of stoichiometric mixture can be introduced and the flamelet equations can be derived. A transformation from the physical spatial-temporal space to a space in which the mixture fraction is introduced as a new independent variable can be done. Thus, the new coordinate is locally attached to an iso-surface of the mixture fraction, say the stoichiometric mixture fraction Z_{st}, and the new coordinates Z_2 and Z_3 lie within this surface [12]. A Crocco-type coordinate transformation is performed and the transformation rules are systematically applied to the governing equations for species and energy [5, 6, 9, 11]. A one-dimensional behaviour in the flame front is assumed at this point. Terms corresponding to gradients along the flame front (gradients along Z_2 and Z_3)

are neglected in comparison to the terms normal to the flame (gradients along Z). Assuming a unity mixture fraction Lewis number Le_z, constant Lewis number for each species Le_i and negligible Soret effect, flamelet equations can be written as [11, 13, 14]:

$$\rho\frac{\partial Y_i}{\partial \tau} = \frac{\rho\chi}{2Le_i}\frac{\partial^2 Y_i}{\partial Z^2} + \frac{1}{4}\left(\frac{1}{Le_i} - 1\right)\left[\frac{\partial \rho\chi}{\partial Z} + \rho\chi\frac{c_p}{\lambda}\frac{\partial}{\partial Z}\left(\frac{\lambda}{c_p}\right)\right]\frac{\partial Y_i}{\partial Z} + \dot{w}_i \tag{3.2}$$

$$\rho\frac{\partial T}{\partial \tau} = \frac{\rho\chi}{2}\frac{\partial^2 T}{\partial Z^2} + \frac{\rho\chi}{2c_p}\frac{\partial c_p}{\partial Z}\frac{\partial T}{\partial Z} + \frac{\rho\chi}{2c_p}\sum_{i=1}^{N}\left(\frac{c_{p_i}}{Le_i}\frac{\partial Y_i}{\partial Z}\right)\frac{\partial T}{\partial Z} - \frac{1}{c_p}\sum_{i=1}^{N} h_i\dot{w}_i + \frac{Q_R}{c_p} \tag{3.3}$$

where T is temperature; c_{p_i} specific heat of ith species; h_i enthalpy of ith species; $\dot{w}_i$ net rate of production of ith species; Y_i mass fraction of ith species; Q_R the radiating heat loss; Le_i is the Lewis number of ith species defined by: $Le_i = \lambda/(\rho\mathcal{D}_{im}c_p)$, being $\mathcal{D}_{im}$ the multicomponent ordinary diffusion coefficients. In these equations χ is the instantaneous scalar dissipation rate defined by:

$$\chi = 2D_z\left(\nabla Z \cdot \nabla Z\right) \tag{3.4}$$

Equations 3.2 and 3.3 are usually simplified assuming negligible: the second term on the r.h.s of Eq. 3.2; the term that involves the Z-derivative of the heat capacity; and the differential diffusion term of Eq. 3.3. Under these simplifications the equations are written as follows:

$$\rho\frac{\partial Y_i}{\partial \tau} = \frac{\rho\chi}{2Le_i}\frac{\partial^2 Y_i}{\partial Z^2} + \dot{w}_i \tag{3.5}$$

$$\rho\frac{\partial T}{\partial \tau} = \frac{\rho\chi}{2}\frac{\partial^2 T}{\partial Z^2} - \frac{1}{c_p}\sum_{i=1}^{N} h_i\dot{w}_i + \frac{Q_R}{c_p} \tag{3.6}$$

For the energy equation, although the term that involves the Z-derivative of the heat capacity is sometimes retained [15–18], the most common formulation do not account for this term [5, 6, 8, 19–21]. Furthermore, often flamelet model calculations are used with the assumption of unity-Lewis number for all species and, therefore, some of the terms that not appear in equations 3.5 and 3.6 directly vanish from equations 3.2 and 3.3.

In this paper, the formulation based on Eq. 3.2 and 3.3 is referred to as **complete equations** formulation (**CE**) while the formulation based on Eq. 3.5 and 3.6 is referred to as **simplified equations** formulation (**SE**)

Given a chemical mechanism, appropriate boundary conditions and scalar dissipation rate profiles $\chi(Z)$, flamelet equations (Eq. 3.2 and 3.3 for CE and Eq. 3.5 and 3.6 for SE) can be integrated to obtain univocal relations for the evaluation of species mass fractions and temperature distributions:

$$\begin{aligned} Y_i &= Y_i(Z,\chi) \\ T &= T(Z,\chi) \end{aligned} \tag{3.7}$$

3.2.3 Scalar dissipation rate modelling

An important quantity in non-premixed combustion is the instantaneous scalar dissipation rate defined by Eq. 3.4, and specially the scalar dissipation rate at stoichiometric conditions denoted by χ_{st}. This is an essential non-equilibrium parameter since it measures the degree of departure from the equilibrium state. In the limit of "fast chemistry" the formulation is reduced introducing $\chi_{st} \longrightarrow 0$. Once the mixture fraction field is known by means of the solution of Eq. 3.1, χ can be calculated at each location of the flow field. Diffusive fluxes arising from spatial gradients are described as a function of the gradients of the mixture fraction Z, and hence the influence of the flow field on the flamelet structure is completely represented by this parameter [11]. It has the dimension $1/s$ and may be interpreted as the inverse of a characteristic diffusion time.

Arising from the flamelet formulation described, a key difficulty to integrate the flamelet equations is to know a priori information about the scalar dissipation rate dependence of the mixture fraction $\chi(Z)$. Flamelet libraries are usually computed in advance and are assumed to be independent of the flow. In this case, the scalar dissipation rate can not be taken from the flow field calculation and has to be introduced as a scalar parameter. Therefore, the scalar dissipation rate dependence of mixture fraction has to be modelled [11].

Different modelizations are reported in the literature to integrate the flamelet equations [5, 21, 22]. In this work the following ones have been considered:

- **Criterion χ_1**: Use of an **analytical approximation** based on the counter-flow diffusion flame or the one-dimensional laminar mixing layer reported in [5, 9]:

$$\chi = \chi_{st} \frac{\Phi}{\Phi_{st}} \frac{f(Z)}{f(Z_{st})} \qquad \text{with} \qquad \Phi = \frac{3}{4} \frac{\left(\sqrt{\rho_\infty/\rho}+1\right)^2}{2\sqrt{\rho_\infty/\rho}+1} \tag{3.8}$$

  where Z_{st} is the stoichiometric mixture fraction; Φ is a factor introduced in order to consider variable density effects [23]; the subscript ∞ means the oxidizer stream and $f(Z)$=exp $\left[-2\left[erfc^{-1}\left(2Z\right)\right]^2\right]$, where $erfc^{-1}$ is the inverse of the complementary error function.

  Using this expression in the flamelet equations, the flamelet library is built with two input parameters: Z and χ_{st}. The scalar dissipation rate at the stoichiometric conditions is evaluated where Z=Z_{st}. With this approach, the functional dependence of the scalar dissipation rate with the mixture fraction $\chi(Z)$ is parameterised by χ_{st}. This value acts as an external parameter that is imposed on the flamelet structure by the mixture fraction field [9]. A set of discrete values of χ_{st} are used from equilibrium (χ_{st}=0) to a quenching value (χ_{st}=χ_q).

- **Criterion $\boldsymbol{\chi_2}$**: Use a **constant** scalar dissipation rate at stoichiometric conditions [19, 20, 24]: $\chi = \chi_{st}$.
- **Criterion $\boldsymbol{\chi_3}$**: Use an **interactive strategy** incorporating the local profile of the scalar dissipation rate at each location of the flame. In this approach, the flamelet library is not only calculated in advanced, but recalculated iteratively with in situ information about the scalar dissipation field calculated in the actual flame simulation. A first solution of the CFD simulation of the flame is obtained considering non-interactive criteria. In this work, the analytical approximation $\boldsymbol{\chi_1}$ is used. Thus, the profile of the scalar dissipation rate $\chi(Z)$ at each position is used to create a new flamelet library. With this library, the CFD simulation is computed again. This process is repeated until convergence is reached. Even though this strategy requires recurrent calculation of the flamelet libraries and the CFD simulation, it allows to include in situ profiles of the scalar dissipation rate of the actual flame solved. On the contrary, this advantage can also be viewed as a penalization due to the loss of generality of the flamelet library since it is generated for a specific situation.

In order to evaluate the scalar dissipation rate at stoichiometric conditions, a discussion is performed when multidimensional flames are simulated. The evaluation of χ_{st} for these flames is not simple, as stoichiometric conditions take place on the flame surface instead of a single point when one-dimensional flames are considered. Therefore, different values of χ_{st} appear along this surface. Given multidimensional flames with parabolic structures of the flow, a common strategy employed in the literature [25] is to evaluate a characteristic χ_{st} at each height position of the flame. At each height, the location of the stoichiometric mixture fraction (i.e. Z_{st}=0.055 for methane flames) is found and χ_{st} is calculated there with Eq. 3.4. This value is used for all the radial positions of that specific height. Downstream the front-flame where no radial position with Z=Z_{st} exists, the centerline value of χ is used as χ_{st}. In the interactive strategy $\chi(Z)$ is taken from the CFD simulation at each flame height.

3.2.4 Steady and Unsteady Laminar Flamelet Models.

In the previous section, the importance of the proper modelling of the scalar dissipation rate dependence of the mixture fraction has been described. The profile employed can influence the flamelet solution significantly. However, even with a proper modelling of the the scalar dissipation rate dependence of the mixture fraction, the chemical flamelet structure cannot follow rapid changes of the scalar dissipation rate instantaneously.

A wide spread approximation is to consider transient effects negligible and, therefore, use the so-called **Steady Laminar Flamelet Models** (**SLFM**) [8, 19–21, 26].

This hypothesis assumes that the flamelet lifetime is much longer than the characteristic time scale of the phenomena involved in the flamelet equations and, as a consequence, the transient terms can be neglected. On the other hand, and in order to take into account rapid changes of the scalar dissipation profiles at the flame front and slow processes as radiation heat transfer or pollutant formation, the unsteady term in the flamelet equations ($\frac{\partial}{\partial \tau}$) must be retained leading to slow relaxation of the profiles [9]. When differential diffusion is considered, it is shown that the transient effect is important in order to balance the term in the flamelet equations responsible of *super-equilibrium* ($\frac{\partial \rho \chi}{\partial Z}$). Inclusion of these transient effects lead to what are known as **Unsteady Laminar Flamelet Models** (**ULFM**) [13, 15, 22, 25, 27].

An illustrative example of the use of unsteady flamelets is the work of Pitsch et. al [22], where a comparison of the characteristic time-scales along the centerline of a diffusion turbulent flame is done. A flamelet lifetime t, a diffusion time t_χ and a characteristic radiation time t_{rad} are defined. They encountered that after some time (30ms in the studied flame), the characteristic diffusion time is longer than the flamelet lifetime and increases rapidly in the following. The effect of radiation is discussed similarly. Furthermore, the flamelet that is transported downstream has to undergo strong changes of χ. Along the axis χ decreases with z^{-4}, being z the distance from the nozzle [22].

In order to use unsteady flamelet modelling, a Lagrangian type flamelet lifetime τ is required to integrate the flamelet equations and, as a result, account for history effects in the flamelet structure. This approach corresponds to a Lagrangian treatment of the flamelet development and is called by some authors as the Lagrangian Flamelet Model to distinguish it from models applied to unsteady flow situations [25]. This characteristic residence time should be evaluated knowing information about the velocity at which a flamelet is transported along the flame. Thus, information of the transport velocity is required in situ. The flamelet time is computed by integration of the inverse of a representative velocity along the stream-wise direction.

A method for parabolic flows is presented hereafter [16]. The flamelets are assumed to be introduced in the flow field at the nozzle exit [25]. From there, they travel downstream with the axial velocity. In order to calculate the Lagrangian type flamelet time τ at each height position z, the relation $v = dz/d\tau$ is used and integrated:

$$\tau(z) = \int_0^z \frac{1}{v(z')} dz' \tag{3.9}$$

The velocity employed in this expression can be calculated, among others, with the following possibilities or criteria:

- **Criterion τ_1**: Use the **stoichiometric velocity**. In the literature, the common approximation is to use the velocity at stoichiometric mixture conditions at each flame height: $v_{Z=Z_{st}}$

- **Criterion τ_2**: Use an **averaged velocity** calculated at each flame height along the radial direction. To avoid an unrealistic low velocity of the flamelet in the flow, the axial area employed to evaluate the average velocity is restricted to the zone where the flame exists. The criterion employed to determine this limit is to consider the average until the mixture fraction is larger than a prescribed value. In this work, the computed area A_z is limited by $Z \geq 10^{-5}$, being the average velocity evaluated as:

$$\langle v(z) \rangle = \frac{1}{A_z} \int_{A_z} v(z) dA'_z \tag{3.10}$$

3.3 Research approach

The aim of the research hereafter presented is to numerically investigate the adequacy of the application of the laminar flamelet concept on the numerical simulation of multidimensional laminar non-premixed flames.

In this investigation, different approaches of the mathematical flamelet formulation described in section 3.2 (viz. flamelet equations, scalar dissipation rate modelling, and the Lagrangian type flamelet time for unsteady flamelets) are taken into account. Numerical solutions obtained assuming laminar flamelet approaches are compared with the numerical solutions obtained from the full resolution of the transport equations (these solutions are hereafter considered as reference solutions). Special attention is given to the prediction of pollutant formation.

3.3.1 Test case

The test case selected is a confined co-flow axisymmetric non-premixed methane/air flame [1, 2]. A stream of pure methane ($\dot{m}_{CH_4} = 0.2165$ g/min) is injected through the inner tube, while a stream of "regular" air ($\dot{m}_{air} = 51.88$ g/min) is injected through the outer tube surrounding it. The stoichiometric mixture fraction has been considered as $Z_{st} = 0.055$. See more details in [3, 4].

The specified boundary conditions are described in [4]. Special attention has been paid to the inlet conditions to relate these values with the known values at the bottom of the burner (this position is hereafter indicated with the subindex B (see [4] for details)). An analogous reasoning as described in [4] for the species and the energy equation, has been followed for the mixture fraction equation at the inlet:

$$(\rho v_z Z)_B = \left[\rho v_z Z - \rho D_z \frac{\partial Z}{\partial z} \right]_{z=0} \tag{3.11}$$

The adequacy of these boundary conditions has been tested using the experimental

data provided by McEnally et. al [1, 28], and also reported by Bennet et. al [2]. The results of this study has been published in [4, 29].

3.3.2 Methodology

Simulation approaches

- **Full-calc**: Detailed simulations based on the full resolution of the transport equations presented in [3, 4] are considered as the *reference* solutions for the validation process. The fluid flow and heat and mass transfer phenomena of the reactive gas is assumed to be described by the governing equations for low-Mach number flows (continuity, species, momentum, energy and state equation).

- **Flamelet modelling simulations**: The fluid flow is calculated with the continuity and momentum equations. The mixture fraction equation is solved and the scalar dissipation rate evaluated. Species and temperature are obtained from the flamelet libraries.

  Steady (SF) vs. unsteady (UF) flamelet modelling are considered. Complete (CE) and simplified (SE) flamelet equations are taken into account (see section 3.2.2). Unsteady flamelets are calculated with the complete flamelet equations (CE) since, in general, the study presented for steady flamelets reveal that taking into account the term that involves the Z-derivative of the heat capacity and the differential diffusion term are of significant importance. Regarding the scalar dissipation rate modelling, the three possibilities described in section 3.2.3 are compared ($\boldsymbol{\chi_1}$,$\boldsymbol{\chi_2}$,$\boldsymbol{\chi_3}$). Finally, a Lagrangian type flamelet time is required to account for flamelet transient effects. The two strategies proposed in section 3.2.4 are examined ($\boldsymbol{\tau_1}$,$\boldsymbol{\tau_2}$). See table 3.1 for more details about the model combinations tested.

Mathematical sub-models

Thermo-physical properties are evaluated using the thermodynamic data compiled in [30]. Transport coefficients of the molecular fluxes of momentum, heat and mass are evaluated considering a mixture-averaged formulation. Pure-species transport properties are evaluated using CHEMKIN's database [31]. For the mixture-averaged viscosity and the thermal conductivity, the semi-empirical Wilke (1950) formulae, modified by Bird (1960) is used [32]. Mixture diffusion coefficients $\mathcal{D}_{im}$, are calculated considering two possibilities based on the definition of the Lewis number:

- Assuming a constant Lewis number for each species, e.g.: $Le_{CH_4} = 0.97$, $Le_{O_2} = 1.11$, $Le_{H_2} = 0.3$. See [4] for details.

Transient effects	Alternatives $Form.$	χ	τ
SF	CE	χ_1	
	CE	χ_2	
	SE	χ_1	
	SE	χ_2	
UF	CE	χ_3	τ_2
	CE	χ_3	τ_1
	CE	χ_1	τ_2

Table 3.1: Summary of the flamelet model approaches used considering: transient effects (SF,UF), flamelet equations formulation (CE,SE), scalar dissipation rate modelling ($\boldsymbol{\chi_1}$,$\boldsymbol{\chi_2}$,$\boldsymbol{\chi_3}$), and the Lagrangian type flamelet time ($\boldsymbol{\tau_1}$,$\boldsymbol{\tau_2}$). See section 3.2 for acronym description.

- Assuming a unity Lewis number for all the species involved in the chemical model ($Le_i = 1.0$, $i = 1, 2, ...N$).

The detailed chemical mechanism considered is the GRI-Mech 3.0 [30], which involves 325 reactions and 53 species. This mechanism is suitable for the description of pollutant formation because it includes NO_x reactions.

Flame radiation is modelled using the assumption of optically thin transfer between the hot combustion gases and the cold surroundings [4, 33, 34]. The definition of an optically thin gas establishes that self-absorption is negligible compared to emission. The radiating species considered in order of importance are CO_2, H_2O, CH_4 and CO. From running RADCAL [35], Planck-mean and incident-mean absorption coefficients, which are fitted to polynomial expressions [33], are obtained at different temperatures.

3.4 Numerical methodology

The mathematical model is discretized using the finite volume technique over cylindrical staggered grids. Central differences are employed for the evaluation of the diffusion terms, while third-order bounded schemes are used for the evaluation of the convective ones [36]. A time-marching SIMPLE-like algorithm is employed to couple velocity-pressure fields [37]. Discretized equations are solved in a segregated manner using a multigrid solver [38]. The convergence of the time-marching iterative procedure is truncated once normalised residuals are below 10^{-8}.

Domain decomposition method is used as a strategy to reduce the number of grid nodes far from the flame fronts, and as a parallelisation technique. For further details see [3, 39, 40].

The computational domain has been discretized considering several zones with different grid nodes distributions. The number of nodes corresponding to each zone is indicated in terms of a grid parameter n. An h-refinement study is performed with five levels of refinement ($n = 1, 2, 4, 8$ and 16). For example, for the finest discretization level, $n = 16$, 141.856 CVs are employed. The mesh distribution is given in [4] with the corresponding verification analysis.

All the numerical simulations have been performed on a *Beowulf cluster* composed by 40 standard PCs AMD (K7) AthlonXP 2600+ (1938 Mhz) CPU and 1024 Mbytes, with a conventional network.

Flamelet equations are converted into a discretized system using the finite volume technique. On their resolution, an operator-splitting procedure and/or a Damped-Newton method is used to reach steady state solutions [3]. Mixture fraction coordinate is discretized with 160 nodes concentrating the mesh around $Z{=}Z_{st}$. The scalar dissipation rate profile is prescribed depending on the modelization used [14]. When χ_{st} is used as the external parameter, values from $2\text{x}10^{-4}$ up to quenching values $\chi_{st,q}$ are considered. Numerical results are stored in what is usually known as *flamelet libraries*.

3.4.1 Verification of numerical solutions

Numerical results are submitted to a verification procedure in order to establish a criteria on the sensitivity of the simulation to the computational model parameters that account for the discretization: the mesh spacing and numerical schemes. This tool estimates the order of accuracy of the numerical solution (observed order of accuracy p), and the error band where the grid independent solution is expected to be contained (uncertainty due to discretization GCI), also giving criteria on the credibility of these estimations. See [3, 4, 41] for further details about this post-processing procedure.

A verification study of the numerical solutions of detailed simulations (**Full-calc**) was presented in [4]. In this paper the numerical results of the flamelet modelling simulations are submitted to the same verification procedure. Estimations are given for a zone limited by $0 \leq r \leq 1.59\ cm$ and $0 \leq z \leq 20\ cm$, which is in fact the space region that encloses the flame.

Representative results for the case of unity-Lewis number assumption for all species and adiabatic flame conditions are presented in Table 3.2. Steady laminar flamelets (SF) have been selected with the complete flamelet formulation (CE) and and analytical approach for the Z-dependence of the scalar dissipation rate (χ_1). Once a mesh is selected with enough confidence and knowing an estimation of its accuracy,

Steady Flamelet modelling (SF,CE,$\boldsymbol{\chi_1}$). Unity-Lewis ($Le_i = 1$). No-Radiation								
grid						GCI^* [%]		
n	$T_{max,C}$	Hf	EI_{CO}	EI_{NO}	EI_{NO_2}	$v_r^* = v_r/v_{in}$	$v_z^* = v_z/v_{in}$	Z
4	2212	5.98	0.000137	47.430	0.799	$4.8\text{x}10^{-1}$	$1.6\text{x}10^{+0}$	$6.6\text{x}10^{-3}$
8	2206	5.91	0.000136	47.404	0.798	$1.5\text{x}10^{-1}$	$3.5\text{x}10^{-1}$	$1.2\text{x}10^{-3}$
16	2210	5.94	0.000136	47.400	0.798	$6.3\text{x}10^{-2}$	$9.9\text{x}10^{-2}$	$3.0\text{x}10^{-4}$

Table 3.2: Verification of the numerical solutions. Main flame features. (n: grid parameter; $T_{max,C}$ [K]: maximum temperature at the symmetry axis; Hf [cm]: flame height; EI_x: emission index; GCI: Grid Convergence Index).

all the modelling and phenomenological studies presented in later sections are performed with this selected mesh. Thus, the conclusions hereafter showed are assumed to be representative of the rest of simulations. The advantages of this approach were shown by Claramunt et al. [4] using the same co-flow flame and considering different levels of partially premixing.

Table 3.2 shows the verification results for flamelet modelling simulations. Even though information for all dependent variables is available, only main flame features together with GCI values for representative variables are here presented. Both radial and axial velocity components are selected. The mixture fraction variable is also chosen as a key variable since its resolution is responsible of the scalar dissipation rate field by means of its gradient (Eq. 3.4), and also responsible of the temperature and species distributions (Eq. 3.7).

When analysing GCI values, it can be observed that numerical solutions obtained with the third level of refinement ($n = 4$) are accurate enough. For example, the non-dimensional velocity field presents small enough averaged uncertainties: $\pm 0.48\%$ for the radial velocity and $\pm 1.60\%$ for the axial velocity. Uncertainty values smaller than $\pm 0.01\%$ are estimated for the mixture fraction variable, which also indicates a proper behaviour of the variables that depend on the mixture fraction, viz. scalar dissipation rate, temperature, species mass fractions and physical properties. As a result of this verification study, all the simulations hereinafter presented are performed with the third level of refinement ($n = 4$, i.e. 10888 CVs).

Assessment of the interactive process for unsteady flamelets. Influence of the number interactions between the CFD and the flamelet code

The influence of the number of interactions between the CFD code and the flamelet-library generation code when unsteady flamelet modelling is considered is herewith presented. As an illustrative example, flamelet simulations have been performed as-

suming differential diffusion and including radiative heat transfer.

In Table 3.3 the mean and maximum differences in the domain between two consecutive numbers of interactive iterations is presented for the selected situation. The complete flamelet equations (CE), the interactive strategy (χ_3) and the stoichiometric velocity is used to evaluate the flamelet lifetime (τ_1).

Unsteady Flamelet modelling (SF,CE,$\boldsymbol{\chi_3}$,$\boldsymbol{\tau_1}$). Lewis-fixed. Radiation.						
	$v_z^* = v_z/v_{in}$		Z		$T^* = T/298$	
Interactions	Av. [%]	Max. [%]	Av. [%]	Max. [%]	Av. [%]	Max. [%]
1st-2nd	$3.6\text{x}10^{+0}$	$2.4\text{x}10^{+1}$	$1.7\text{x}10^{-3}$	$2.3\text{x}10^{-1}$	$5.2\text{x}10^{-1}$	$9.8\text{x}10^{+0}$
2nd-3rd	$2.2\text{x}10^{-1}$	$1.7\text{x}10^{+0}$	$1.2\text{x}10^{-4}$	$2.1\text{x}10^{-2}$	$2.5\text{x}10^{-2}$	$8.6\text{x}10^{-1}$
3rd-4th	$2.8\text{x}10^{-2}$	$2.0\text{x}10^{-1}$	$1.6\text{x}10^{-5}$	$2.5\text{x}10^{-3}$	$3.3\text{x}10^{-3}$	$9.7\text{x}10^{-2}$
	Y_{CO}		Y_{NO}		Y_{NO_2}	
Interactions	Av.[%]	Max.[%]	Av.[%]	Max.[%]	Av.[%]	Max.[%]
1st-2nd	$3.6\text{x}10^{-3}$	$3.4\text{x}10^{-1}$	$3.6\text{x}10^{-7}$	$3.5\text{x}10^{-3}$	$2.6\text{x}10^{-8}$	$5.5\text{x}10^{-5}$
2nd-3rd	$1.3\text{x}10^{-4}$	$1.5\text{x}10^{-2}$	$3.7\text{x}10^{-8}$	$1.3\text{x}10^{-4}$	$1.3\text{x}10^{-9}$	$5.1\text{x}10^{-6}$
3rd-4th	$1.3\text{x}10^{-5}$	$1.8\text{x}10^{-3}$	$4.3\text{x}10^{-9}$	$1.7\text{x}10^{-5}$	$1.4\text{x}10^{-10}$	$5.3\text{x}10^{-7}$

Table 3.3: Mean and maximum differences between two consecutive interactions between the CFD code and the flamelet code generation. Unsteady Flamelet modelling with differential diffusion ($Le_i = ct$), radiation, χ_3 criterion and τ_1 criterion.

This table reveals that the differences between the numerical solutions obtained after the first and the second interaction between the CFD and the flamelet code are still too large, but the differences between the second and the third interaction are small enough to ensure an accurate result. The averaged temperature difference between the second and the third interactions is about 0.025%. The dimensional value of this difference means approximately $\pm 0.07K$. The maximum difference of the temperature field is less than 1%. Not only does the temperature have little differences between the second and the third interaction, but also the mixture fraction, the axial velocity and the main pollutant species mass fraction (CO, NO and NO_2).

The study performed justifies the use of the second interaction as an accurate enough numerical result. This strategy has been used for all the unsteady flamelet modelling simulations presented in the next section.

3.5 Results and discussion

A detailed analysis of the mathematical flamelet approaches described in this work is discussed in the next subsections. In this discussion, two main kinds of flamelet approaches are distinguished: steady vs. unsteady flamelets. Major differences concerning main flames properties, and specially pollutant formation, have been found to be very sensitive to the consideration of the flamelet approach. The other flamelet model alternatives, i.e. flamelet equations formulation and the influence on the scalar dissipation rate modelling, are being considered in both general approaches to analyse their influence and/or their possible improvements.

Special attention is paid on the influence of including the differential diffusion and/or radiation term in the laminar flamelet equations. To emphasise the appropriateness of the flamelet approaches employed, it has been considered of interest to decouple both effects identifying four different situations: i) unity-Lewis numbers and radiation not included; ii) unity-Lewis numbers and radiation included; iii) fixed-Lewis numbers and radiation not included; iv) fixed-Lewis numbers and radiation included.

Results discussion is supported by table 3.4 and figures 3.2-3.6, where numerical solutions obtained with the different flamelet approaches and models considered are compared with **Full-calc** results. Table 3.4 shows the main flame features for different flamelet modellings compared to the *reference* results simulations (**Full-calc**). Figures 3.2-3.4 show the centerline profiles of temperature and mass fraction of CO and NO for all the phenomenological situations described above. Figure 3.5 shows the temperature radial profiles at three different heights (10, 50 and 100 mm) for adiabatic flame consideration with and without differential diffusion. Finally, figure 3.6 shows the radial profile at z=50 mm for temperature and mass fraction of CO, NO and NO_2 considering both radiation heat transfer and differential diffusion effects.

3.5.1 Unity-Lewis and No-Radiation

Steady Flamelets

For the case of Unity-Lewis number and without thermal radiation (adiabatic flame), the temperature is very well approximated to the **Full-calc** simulation with the complete flamelet equations (CE) and are significantly under-predicted when the simplified equations (SE) are considered. The term that involves the Z-derivative of the heat capacity present in equation 3.3 and neglected in 3.6 is responsible of this discrepancy. This term is very important for the appropriate prediction of the temperature in all cases. In the inner flame region the temperature profile is properly described but regarding the temperature peak, its height and the post-flame profile is clearly under-predicted. This tendency is also appreciated in the radial profiles (Fig. 3.5).

On the other hand, the temperature field is not very sensitive to the scalar dissipation rate modelling since the different criteria considered show similar results.

The same trend is followed by the main species distributions (CH_4, O_2, H_2O and CO_2) and also for the majority of radicals (e.g. OH, H, CH_3). On the contrary, species that are slowly produced or consumed are poorly predicted with steady approaches. That is the case of the main pollutant contributors, CO, NO and NO_2.

Figure 3.3 shows that the CO mass fraction profile of the inner flame region and its rapid decrease is properly predicted compared to the **Full-calc** simulation. Even though, the main peak is slightly under-predicted. Nevertheless, CO production/consumption is a slow process and steady flamelets have serious difficulties to describe it. This fact is clearly observed in the emission indexes predictions presented in table 3.4. EI_{CO} is under-predicted three orders of magnitude in the most favourable steady flamelet simulation: 0.00014 compared to 0.27, which is the **Full-calc** result.

Fig. 3.4 shows that the peak centerline NO formation for SF-CE models are almost six times larger than the **Full-calc** profile. For simplified equations (SE) this peak over-prediction reduces to two times. This fact is due to NO is very temperature dependent and a larger temperature produces a larger *thermal* NO formation. The question is not the flamelet equations employed (CE or SE), but the steady flamelet assumption. NO formation is a slow process and is not able to undergo the rapid changes of χ, specially in the flame front. At the inner-flame region NO is still well described but near the flame front, and specially in the post-flame region, this prediction gets worse. Emission index of NO, is one order of magnitude over-predicted with steady flamelets.

The emission index of NO_2 is not so affected by steady flamelets assumption, although it is over-predicted with a factor of two when the complete flamelet equations are used (CE), and it is slightly under-predicted with simplified flamelet equations (SE). The behaviour of the emission indexes is a consequence of the mass fraction radial profiles at the upper region of the flame.

Unsteady Flamelets

When a unity-Lewis number is assumed and radiation is neglected, the temperature, major species involved in the chemical mechanism employed for methane/air combustion (i.e. CH_4, O_2, CO_2, H_2O), and most of the secondary species do not have a significant improvement when unsteady flamelet approach is used. These variables are not involved in slow processes, thus transient effects are negligible to be able to properly predict them with the flamelet approach.

On the other hand, the emission indexes of pollutant species are clearly improved when unsteady flamelets are used. For both scalar dissipation rate modelling (χ_1 and χ_3) this improvement is appreciated, specially for the interactive strategy χ_3. When the averaged velocity (τ_2) is taken into account the emission indexes are closer

to the **Full-calc** results. This indicates that the stoichiometric velocity τ_1 tends to under-predict the residence time of the flamelet inside the domain.

Figure 3.1 shows an example of the velocity and the flamelet lifetime. A comparison of these profiles is shown when a **stoichiometric velocity** or an **averaged velocity** is used. The stoichiometric velocity is larger than the averaged velocity, specially in the post-flame region because the centerline profiles are selected as the characteristic velocity when τ_1 is considered. Obviously, these velocity profiles produce an inverse behaviour of the flamelet lifetime. This means that with a larger velocity, the lower flamelet lifetime is found. The behaviour of the unsteady flamelets is very sensitive to the flamelet lifetime considered.

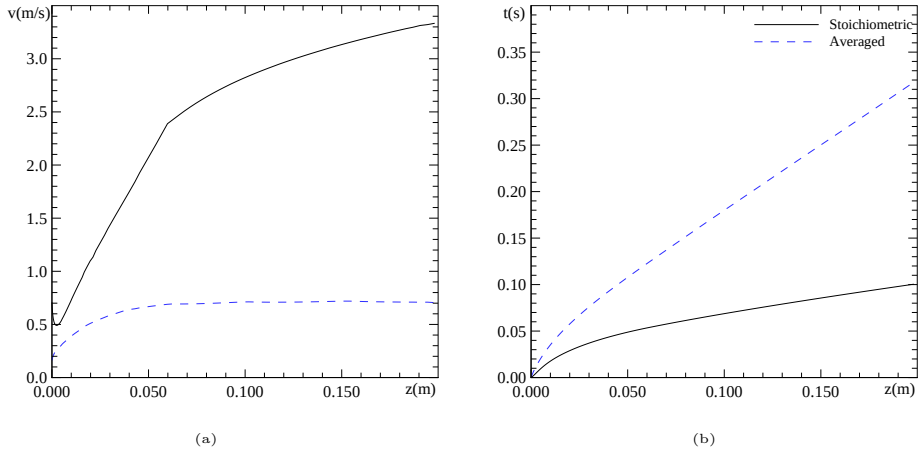

Figure 3.1: Velocity and flamelet lifetime profiles along the centerline for co-flow methane/air laminar flame. Unity-Lewis and No-radiation: (a) velocity; (b) flamelet lifetime.

CO centerline profile is slightly better predicted with the unsteady flamelet assumption, the interactive strategy for the scalar dissipation rate modelling (χ_3) and the stoichiometric velocity (τ_1) (see Fig. 3.3). Otherwise, the radial profiles of CO mass fraction reveal that at the inner-flame zone and up to the height of the flame, all unsteady models properly predict this species. However, at the post-flame zone, the use of a stoichiometric velocity produces a significant over-prediction of the CO radial profile. That explains the results of the emission indexes.

A similar behaviour is observed by NO mass fractions. This pollutant is properly improved by all the unsteady approaches, even though the post-flame region is better predicted when the averaged velocity (τ_2) is considered. EI_{NO} estimation is substan-

tially improved by the unsteady flamelet simulations compared to steady approaches. See for example that UF-CE-χ_3-τ_2 predicts an $EI_{NO} = 6.81$ and the **Full-calc** results is 5.72.

NO_2 mass fraction and its emission index is slightly better predicted with the averaged velocity (τ_2) and the interactive strategy for the scalar dissipation rate modelling (χ_3). That trend is clearly defined as the post-flame region is reached.

3.5.2 Unity-Lewis and Radiation

When radiation heat transfer is included, each flamelet has two quenching limits. One of them takes place for large χ_{st} because the heat release rate cannot equilibrate the large conduction that this large χ_{st} implies. This is caused by the over-stretching of the flame. At high dissipation rates, the high stretching in the flame causes high diffusion rate of species, and more fuel and oxygen penetrate each other, which leads to an incomplete reaction [20]. Flame radiation can induce another extinction limit at a low scalar dissipation rate since in this limit, the influence of radiation heat loss becomes significant. At a very low scalar dissipation rate, the combustion temperature is reduced due to the radiation heat loss, which results in a lower reaction rate and higher reactant leakage [20].

Steady Flamelets

In general, steady flamelet models are unable to reproduce an adequate temperature level since an over-estimation of the radiation heat loss is produced. As a consequence, temperature dependent species are also not properly described. The height of the flame is slightly over-predicted for all steady flamelet approaches with respect to the **Full-calc** simulation. This confirms that the inclusion of radiation with steady flamelets produces unrealistic results [16].

Assuming steady flamelets (SF) with complete flamelet equations (CE) and analytical modelling of the scalar dissipation rate (χ_1), the peak temperature at centerline differs with respect to **Full-calc** approximately $260K$. If simplified flamelet equations (SE) are employed this difference increase until $330K$ (see table 3.4 and figure 3.2). The quenching limit for low scalar dissipation rates produces this significant under-prediction of temperature at this point and, as a consequence, of CO and NO mass fractions (see Figs. 3.3 and 3.4). This effect is specially important around Z_{st}. At the flame front it is where the main differences are found. Temperature-dependent species (eg. NO) are very affected by the low temperatures predicted.

Figure 3.3 shows for all steady flamelet approaches that at the centerline CO is under-predicted in the inner-flame region, but this tendency is inverted when the mixture fraction is lower than the stoichiometric value, producing the large EI_{CO} found. EI_{CO} is one order of magnitude over-predicted when CE and the analytical

scalar dissipation rate modelling (χ_1) is employed, and two orders of magnitude when the constant scalar dissipations rates are used (χ_2). NO is under-predicted along the centerline and EI_{NO} is under-estimated. Even though, variables close to the nozzle are properly described, specially for CE and χ_1. Concerning EI_{NO_2}, it is well predicted by χ_1 but half predicted by χ_2.

Unsteady Flamelets

Unsteady flamelets clearly contribute to a proper description of the flame in non-adiabatic conditions and very close results to the **Full-calc** simulation are obtained. Radiation heat transfer involve a characteristic time scale slower than the flamelet lifetime, at least in some zones of the flame domain. Therefore, unsteady flamelets allow to account for the important transient effects involved.

Temperature centerline profile (Fig. 3.2) experiments a clear improvement specially when the stoichiometric velocity (τ_1) is considered for the evaluation of the flamelet residence time. The averaged velocity (τ_2) produces a larger residence time that over-estimates the effect of the transient effect.

Using the interactive approach for the scalar dissipation rate modelling (χ_3), CO mass fraction is also better predicted when τ_1 approach is employed at the inside-flame region, but this effect is not maintained in the post-flame region. Thus, CO profile is slightly over-predicted for τ_1 approach and it is more accurately predicted by τ_2. This is also reflected in EI_{CO}.

EI_{NO} is not so sensitive to the residence flamelet time adopted. Both NO profiles obtained with τ_1 and τ_2 are well predicted. On the other hand, the description of NO_2 formation is also slightly better performed by τ_1.

In conclusion, all unsteady models clearly enhance the poor results of the steady flamelet models referring to the temperature and the pollutant formation. The interactive strategy χ_3 has a slightly better performance than the analytical approximation χ_1. Furthermore, the evaluation of the flamelet lifetime is revealed as having a strong influence, being the stoichiometric velocity criterion τ_1 more appropriate in this case.

3.5.3 Fixed-Lewis and No-Radiation

Differential diffusion is one of the most difficult phenomena to be accounted for the flamelet modelling simulations. Species equation of the complete flamelet equations (Eq. 3.2) includes a term that only exists when the Lewis numbers are different from unity. This term is a key contributor to the behaviour of the flamelet modelling simulations when differential diffusion is considered.

The consideration of the derivative of the scalar dissipation rate with the mixture fraction ($\frac{\partial \rho \chi}{\partial Z}$) produces an imbalance of the equilibrium chemistry for low scalar dissipation rates, which is called *super-equilibrium*. When $\chi \to 0$ the flamelet equations

should reduce to equilibrium, except for this term.

Steady Flamelets

In general, steady flamelets properly describe the temperature close to the nozzle, but the great differences are found as the front-flame region is reached and specially at the post-flame zone.

The flamelet equations employed and the scalar dissipation rate modelling strongly affect the simulations, as the term $(\frac{\partial \rho \chi}{\partial Z})$ that is present in Eq. 3.2 vanishes with χ_2 and is neglected with the simplified equations (SE). Consequently, when this approach is considered and this term is not accounted for, *super-equilibrium* effect is avoided and temperature is not over-predicted. Temperature is about $135K$ lower than the **Full-calc** simulation, although the flame height is still $1.76cm$ higher. Being the NO formation very temperature dependent, it is not so over-predicted.

On the other hand, when the complete flamelet equations (CE) and the analytical expression of the scalar dissipation rate (χ_1) are used, a substantial over-prediction of temperature profiles, NO and NO_2 mass fractions is observed. Figures 3.2 and 3.5 show the dramatic over-prediction of the flame temperature at the flame front, the over-prediction of the height of the flame and also the post-flame temperature along the centerline. In table 3.4, it is shown that the difference of the peak centerline temperature between the **Full-calc** simulation and the SF-CE-χ_1 is about $245K$, and the flame height is 2.66 cm over-predicted. This tendency is also clearly seen in the radial profiles (Fig. 3.5), particularly in the upper flame position ($z = 100$ mm) of temperature. Thus, CO, NO_2 and NO mass fractions are not properly described, specially NO, which is approximately 25 times larger than the **Full-calc** profile.

With reference to the emission indexes, EI_{CO} is considerably under-predicted while EI_{NO} and EI_{NO_2} are over-predicted. CO is still consumed until it reaches the end of the simulated domain ($z = 200$ mm).

Unsteady Flamelets

It has been shown that differential diffusion is a phenomena that is difficult to be properly captured by steady flamelets. The CE steady flamelet modelling simulations produce a very significant over-prediction of the temperature field. In order to avoid *super-equilibrium*, the second term on the r.h.s of Eq. 3.2 needs to be balanced by the time-derivative term.

The peak temperature at the centerline and the post-flame temperature are clearly improved with unsteady flamelets. This improvement is also appreciated in Fig. 3.5 for the radial profiles. To know in situ information of the scalar dissipation rate profiles (χ_3) is of great importance when differential diffusion is accounted for. Furthermore, the importance of the selection of the characteristic velocity of the flamelet required

to evaluate the residence time is shown in figure 3.2. In this case, the use of a stoichiometric velocity (τ_1) under-estimates the importance of the transient effect because of the little flamelet lifetime that this modelization accounts for. Otherwise, an assumption of a lower velocity (τ_2) provides a larger residence time and, as a consequence, a larger weight of the time-derivative term.

Pollutant formation is also substantially improved. Two main factors can be identified here. First, pollutant formation is temperature-dependent (specially *thermal NO* formation) and a poor prediction of temperature directly implies a poor NO prediction. In this case, the temperature and the pollutant formation are over-predicted. Secondly, and in addition, pollutant formation has a slow time scale and steady flamelets fail in the estimation.

3.5.4 Fixed-Lewis and Radiation

Steady Flamelets

This is the most complex case as it includes both differential diffusion and radiation heat transfer. Steady flamelet slightly over-predicts the flame height (see Fig. 3.2). The peak temperature is under-predicted due to the quenching limit of the flamelet for low scalar dissipation rates when radiation is included. This under-prediction is not as large as it is in the unity-Lewis number case with radiation (e.g. $175K$ for SF-CE-χ_1 case). This is probably due to the fact that the differential diffusion term present in the species equation tends to produce the opposite effect as with radiation, i.e. increasing the temperature.

The CO behaviour is similar to the situation described for unity-Lewis and radiation (see table 3.4, and figures 3.3 and 3.6). The same behaviour described for the unity-Lewis number situation is also found for NO and NO_2.

Unsteady Flamelets

Table 3.4 and figures 3.2-3.4 and 3.6 show that, even though unsteady flamelets improve the results of the steady flamelet models, the centerline temperature is not accurately predicted compared to **Full-calc** simulations. The inner-flame region is properly predicted but close to the front-flame and specially in the post-flame region, flamelet models differ from the **Full-calc** simulations. The use of an averaged velocity (τ_2) under-predicts the peak flame and a stoichiometric velocity (τ_1) over-predicts it. An intermediate velocity and, consequently, an intermediate flamelet lifetime could improve the results. This reveals that further investigation is required to model this residence time.

Approach	Alternatives			$T_{max,C}$	Hf	T_{max}	(r,z)	EI_{CO}	EI_{NO}	EI_{NO_2}
	Form.	χ	τ	$[K]$	$[cm]$	$[K]$	$[cm]$	$[g/kg]$	$[g/kg]$	$g/kg]$
Unity Lewis number ($Le_i = 1$) No-Radiation										
SF	CE	χ_1		2212	5.98	2212	0.00, 5.98	0.00014	47.40	0.80
	CE	χ_2		2213	5.98	2213	0.00, 5.98	0.00110	45.02	0.62
	SE	χ_1		2086	6.27	2086	0.00, 6.27	0.00008	14.10	0.24
	SE	χ_2		2087	6.27	2087	0.00, 6.27	0.00061	13.09	0.22
UF	CE	χ_3	τ_2	2201	5.98	2001	0.00, 5.98	0.44	6.81	0.40
	CE	χ_3	τ_1	2189	5.98	2189	0.00, 5.98	7.46	4.31	1.21
	CE	χ_1	τ_2	2195	5.98	2195	0.00, 5.98	1.94	4.75	1.13
Full-calc				2200	5.98	2200	0.00, 5.98	0.27	5.72	0.43
Unity Lewis number ($Le_i = 1$) Radiation										
SF	CE	χ_1		1734	6.56	2012	0.68, 0.22	3.55	1.12	0.43
	CE	χ_2		1643	7.15	1959	0.67, 0.14	10.46	0.67	0.19
	SE	χ_1		1665	6.85	1933	0.68, 0.18	6.71	0.61	0.48
	SE	χ_2		1580	7.45	1890	0.66, 0.07	16.42	0.37	0.18
UF	CE	χ_3	τ_2	1760	5.98	2031	0.68, 0.40	0.66	3.20	0.41
	CE	χ_3	τ_1	1983	5.98	2039	0.68, 0.40	8.18	3.27	1.27
	CE	χ_1	τ_2	1821	5.69	2026	0.68, 0.36	2.41	3.28	1.22
Full-calc				1995	5.98	2047	0.67, 0.53	0.43	4.17	0.46
Differential diffusion ($Le_i = ct$) No-Radiation										
SF	CE	χ_1		2338	8.35	2338	0.00, 8.35	0.0233	151.7	1.87
	CE	χ_2		2082	7.45	2083	0.12, 7.15	0.0019	17.82	0.34
	SE	χ_1		1959	7.45	1959	0.00, 7.45	0.0001	4.51	0.10
	SE	χ_2		1955	7.45	1955	0.05, 7.45	0.0009	3.81	0.13
UF	CE	χ_3	τ_2	2164	5.55	2165	0.05, 5.55	0.15	6.25	0.38
	CE	χ_3	τ_1	2213	6.27	2213	0.00, 6.27	1.60	5.50	0.73
	CE	χ_1	τ_2	2235	6.85	2238	0.12, 6.85	0.75	4.81	0.86
Full-calc				2093	5.69	2093	0.00, 5.69	0.19	4.53	0.41
Differential diffusion ($Le_i = ct$) Radiation										
SF	CE	χ_1		1718	7.15	2000	0.69, 0.28	2.07	0.79	0.36
	CE	χ_2		1549	8.65	1783	0.67, 0.18	20.70	0.31	0.12
	SE	χ_1		1558	8.05	1801	0.68, 0.25	10.99	0.19	0.33
	SE	χ_2		1502	8.95	1748	0.67, 0.18	28.60	0.16	0.09
UF	CE	χ_3	τ_2	1755	5.69	2071	0.70, 0.32	0.24	3.15	0.34
	CE	χ_3	τ_1	1993	6.56	2086	0.71, 0.44	1.84	3.78	0.75
	CE	χ_1	τ_2	1772	6.27	2015	0.68, 0.48	0.97	2.97	0.91
Full-calc				1893	5.98	2009	0.66, 0.66	0.32	3.36	0.44

Table 3.4: Full-calc vs. flamelet modelling simulations. Main flame characteristics. ($T_{max,C}$: maximum temperature at the symmetry axis; Hf: flame height; $T_{max}, (r,z)$: maximum flame temperature and location; EI_x: emission index, defined as the fraction between grams per second of pollutant species and kilograms per second of methane burned).

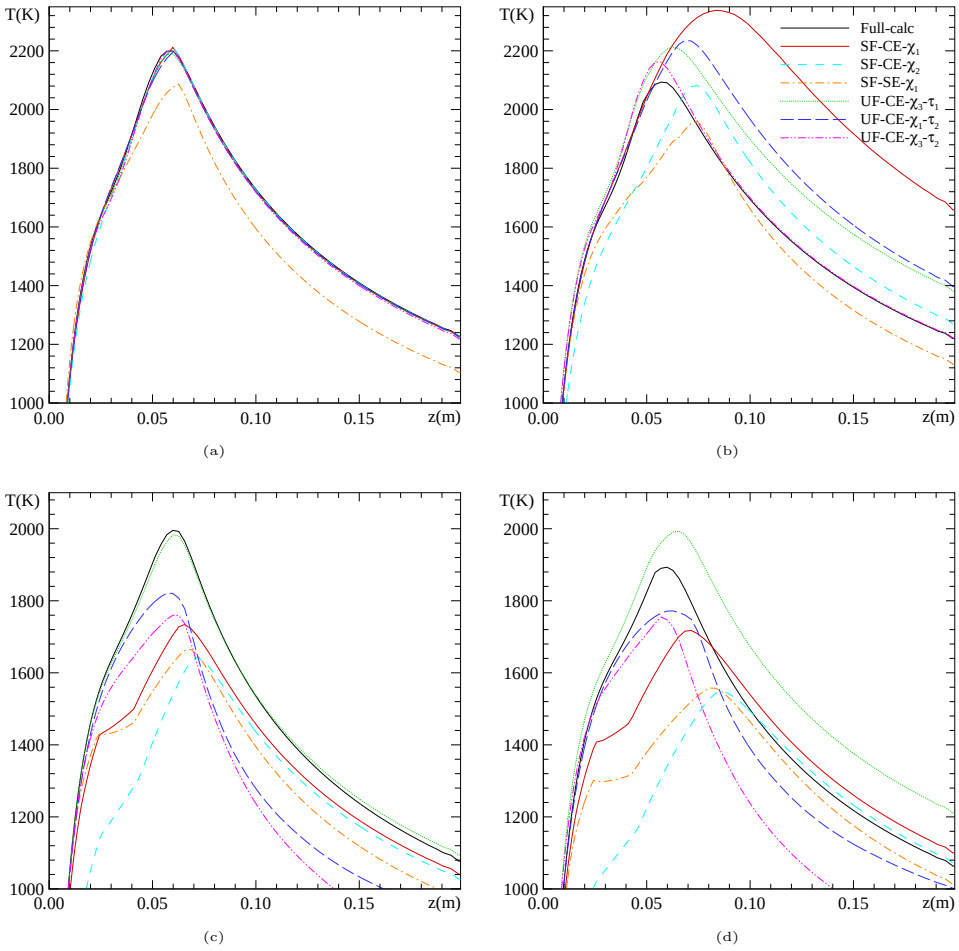

Figure 3.2: Temperature centerline profiles for co-flow methane-air laminar flame: (a) Unity-Lewis and No-radiation; (b) Fixed-Lewis and No-radiation; (c) Unity-Lewis and radiation; (d) Fixed-Lewis and radiation.

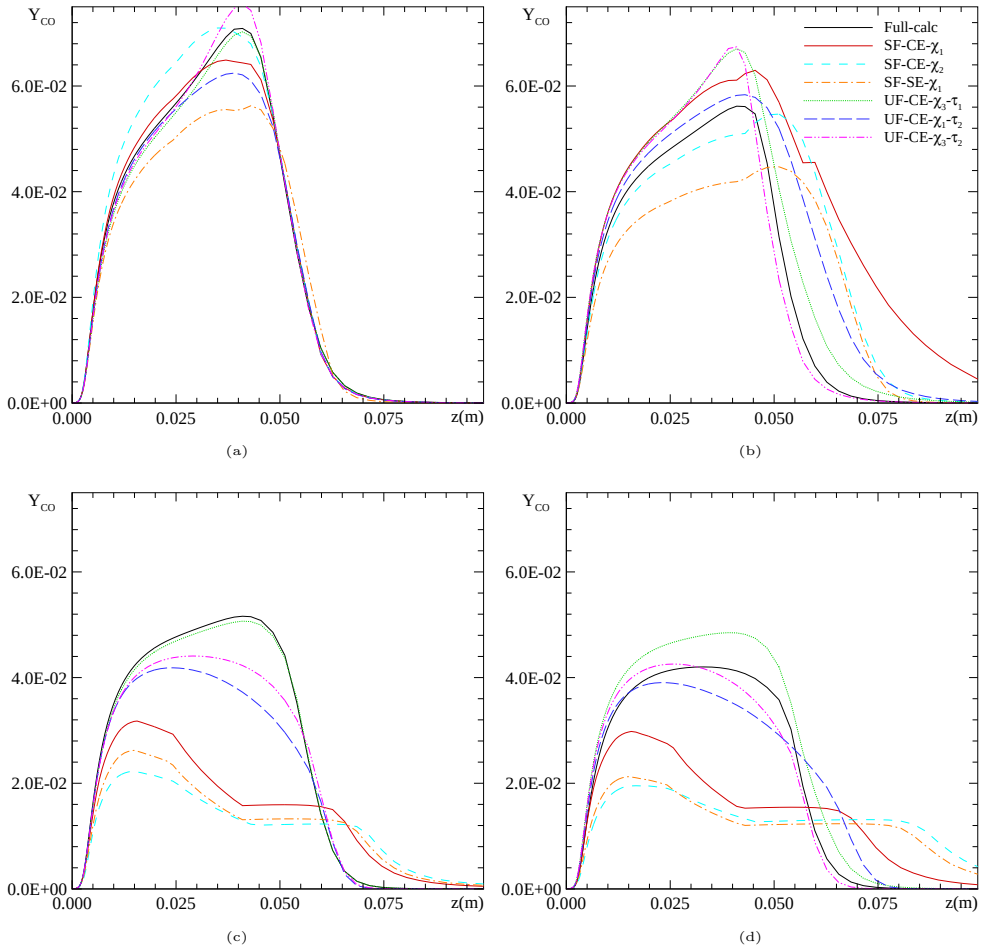

Figure 3.3: *CO* mass fraction centerline profiles for co-flow methane-air laminar flame: (a) Unity-Lewis and No-radiation; (b) Fixed-Lewis and No-radiation; (c) Unity-Lewis and radiation; (d) Fixed-Lewis and radiation.

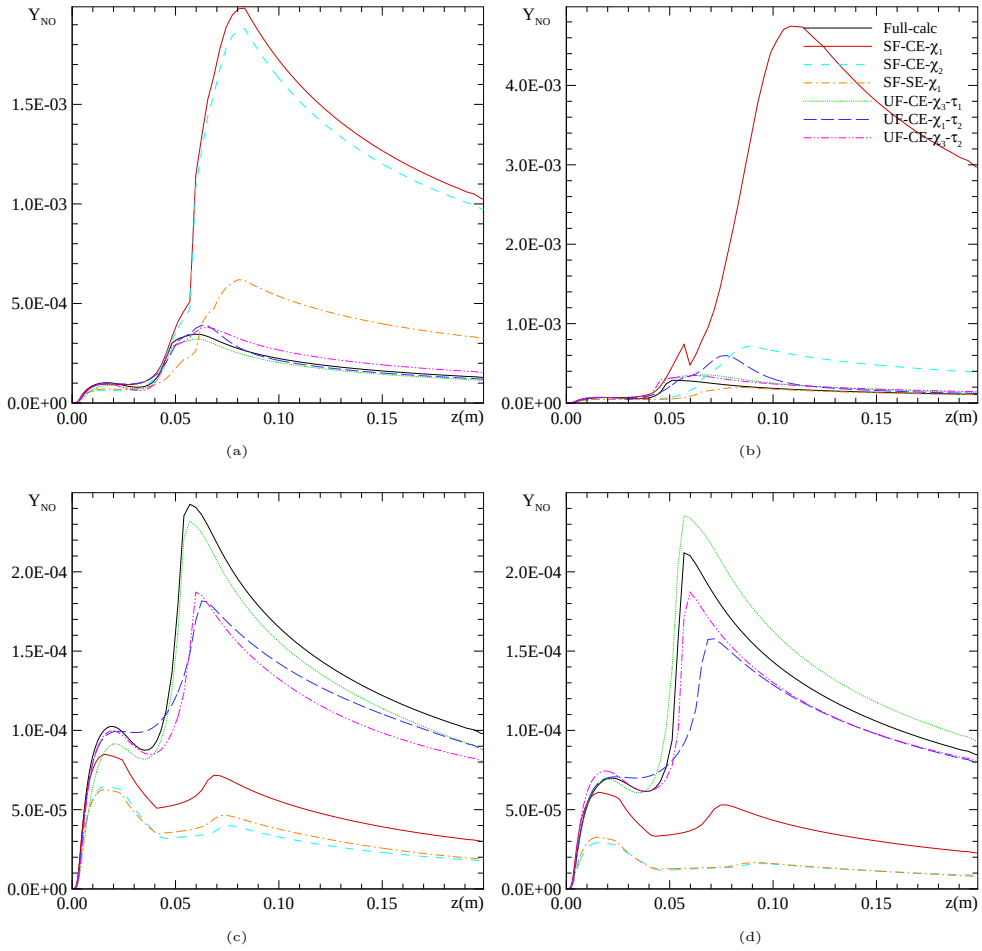

Figure 3.4: *NO* mass fraction centerline profiles for co-flow methane-air laminar flame: (a) Unity-Lewis and No-radiation; (b) Fixed-Lewis and No-radiation; (c) Unity-Lewis and radiation; (d) Fixed-Lewis and radiation.

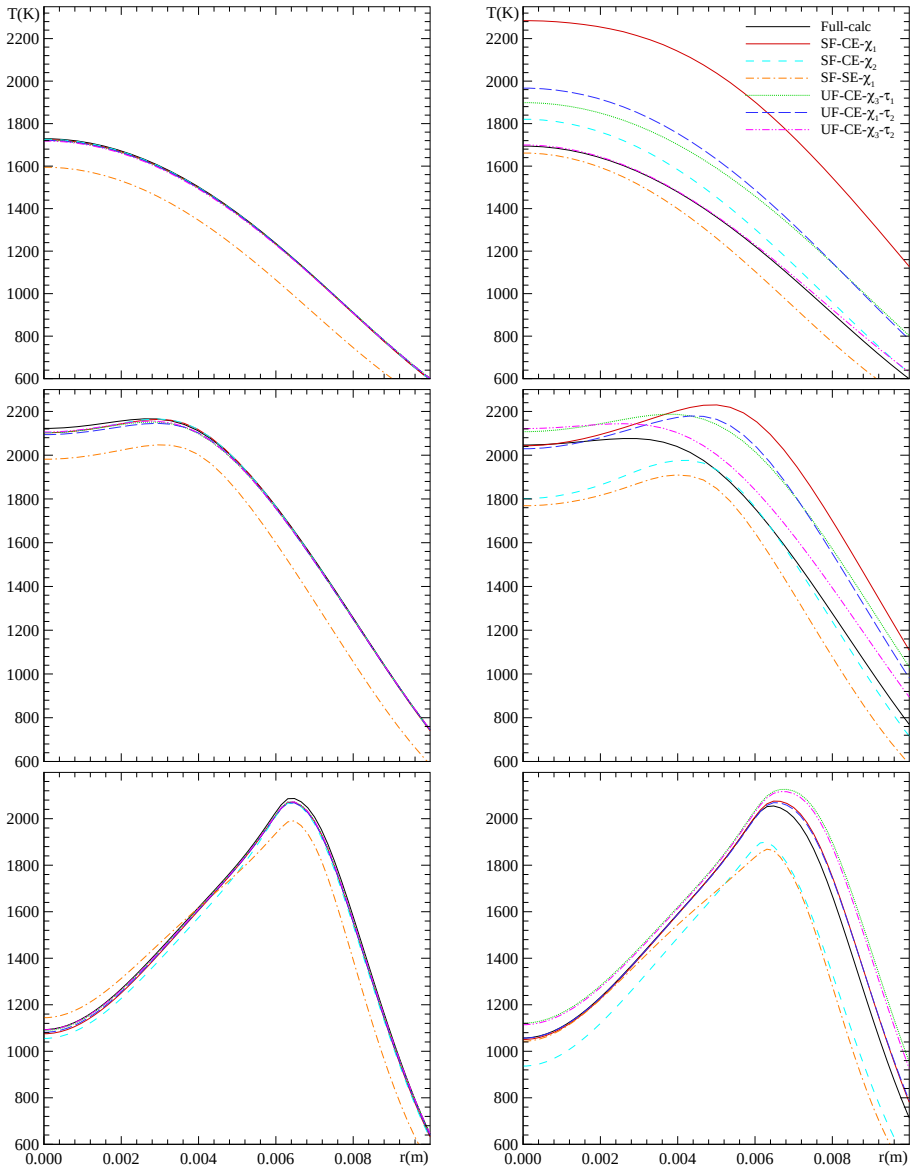

Figure 3.5: Temperature radial profiles for co-flow methane-air laminar flame: No-radiation; (left: Unity-Lewis; right: Fixed-Lewis).

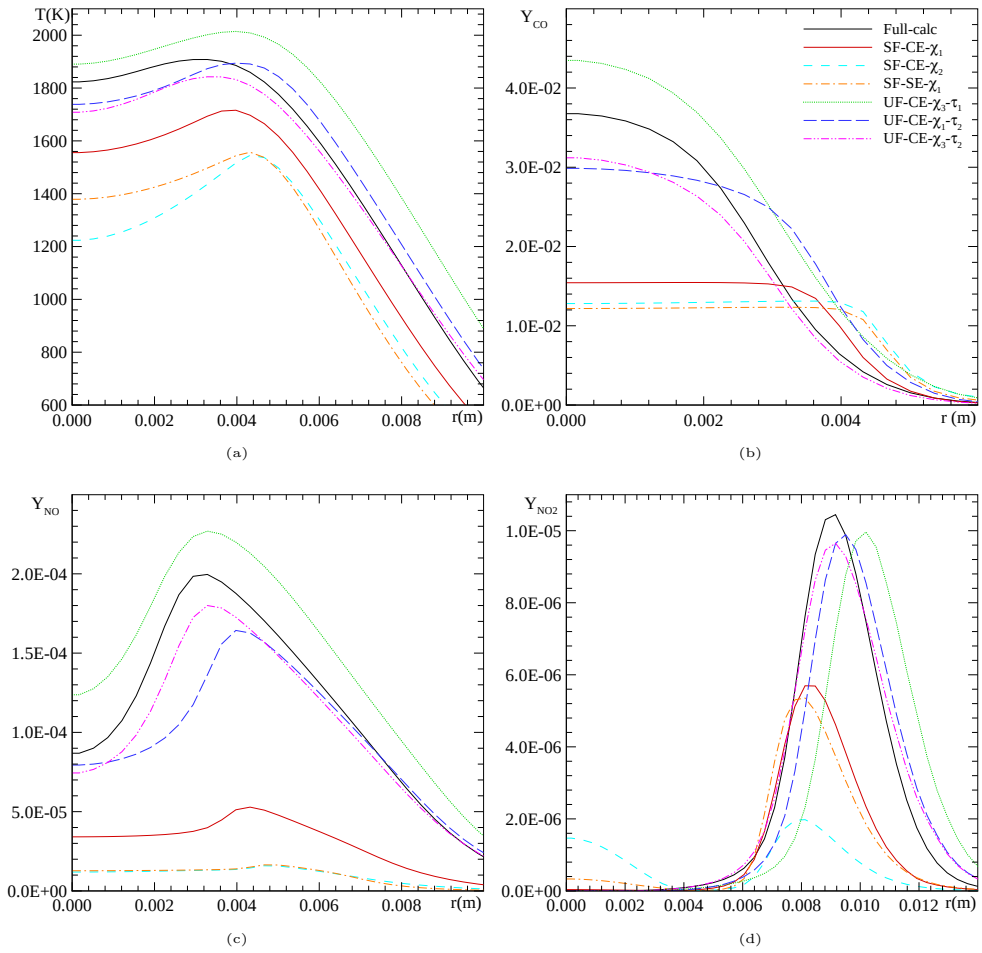

Figure 3.6: Radial profiles for co-flow methane-air laminar flame at z=50 mm. Radiation and Fixed-Lewis: (a) Temperature; (b) CO mass fraction; (c) NO mass fraction; (d) NO_2 mass fraction.

3.6 Conclusions

The adequacy of the application of steady and unsteady laminar flamelet models for the numerical simulation of multidimensional non-premixed laminar flames has

been investigated comparing different flamelet mathematical formulations with the full resolution of the transport equations (**Full-calc**). Special attention has been paid to radiation heat transfer and differential diffusion effects.

When the flame is considered adiabatic and the differential diffusion effect is neglected (Le_i=1), the main flame trends like the temperature field and the main species and the majority of radicals are properly described with steady flamelet simulations. On the contrary, a slow process like pollutant formation (CO, NO and NO_2) and radiation effects are significantly poorly predicted by the steady approach of the flamelet equations. Also, unsteady flamelets have been proved to be very useful in order to avoid the *super-equilibrium* effect when differential diffusion is considered. A noticeable improvement on the main flame features and the axial and radial profiles of temperature and species is observed when unsteady flamelets are used.

The term that involves the Z-derivative of the heat capacity in the energy flamelet equation is an important term in order to properly predict the temperature field and, i.e. consequently, the prediction of the high temperature-dependent species, pollutants. The differential diffusion term in the species flamelet equation is responsible of the *super-equilibrium*. It has been shown that the transient effect is important in order to balance this term.

The scalar dissipation rate dependence on the mixture fraction has been revealed to be a key aspect when flamelet modelling simulations are taken into account. If steady flamelets are considered, the use of an analytical approximation for the counter-flow diffusion flame or the one-dimensional laminar mixing layer clearly improve the results compared to a simple constant scalar dissipation rate at stoichiometric conditions. However, when unsteady flamelets are used, and in situ information of the scalar dissipation rate profiles is available, the interactive strategy is suggested.

Finally, the evaluation of the Lagrangian type flamelet time has been shown to be a relevant issue when unsteady flamelets are taken into account. A characteristic velocity at which a flamelet is transported along the flame is required and two strategies have been compared. The stoichiometric velocity tends to under-predict the flamelet lifetime, specially at the post-flame region. An averaged velocity calculated at each flame height along the radial direction is shorter than the stoichiometric velocity and, as a consequence, the flamelet lifetime is longer. In general, a slight improvement of the unsteady flamelet modelling results is observed when the averaged velocity is used.

In conclusion, steady flamelets show a proper performance to predict the main flame features when differential diffusion and radiation heat transfer are neglected. Otherwise, differential diffusion and slow processes such as radiation or pollutant formation require unsteady flamelet modelling in order to properly capture the flame properties. A complete flamelet equations formulation is revealed to be of great importance to correctly reproduce the main features of the flame and account for

effects such as the heat capacity dependence on temperature, enthalpy interdiffusion and differential diffusion. Furthermore, a proper modelling of the scalar dissipation rate dependence of the mixture fraction and the evaluation of the flamelet lifetime are key aspects of the flamelet simulations. A further study on this matter would be necessary.

Acknowledgements

This work has been financially supported by the Comisión Interministerial de Ciencia y Tecnología, Spain (project TIC2003-07970). Authors also acknowledge the useful suggestions of Prof. J-Y. Chen from the University of California at Berkeley, Prof. R. Viskanta and Prof. J. Gore from Purdue University, and Prof. H. Pitsch from Stanford University.

References

[1] C.S. McEnally and L.D. Pfefferle. Aromatic and linear hydrocarbon concentration measurements in a non-premixed flame. *Combustion Science and Technology*, 116–117:183–209, 1996.

[2] B.A. Bennett, C.S. McEnally, L.D. Pfefferle, and M.D. Smooke. Computational and experimental study of axissymmetric coflow partially premixed methane/air flames. *Combustion and Flame*, 123:522–546, 2000.

[3] R. Cònsul, C.D. Pérez-Segarra, K. Claramunt, J. Cadafalch, and A. Oliva. Detailed numerical simulation of laminar flames by a parallel multiblock algorithm using loosely coupled computers. *Combustion Theory and Modelling*, 7(3):525–544, 2003.

[4] K. Claramunt, R. Cònsul, C.D. Pérez-Segarra, and A. Oliva. Multidimensional mathematical modeling and numerical investigation of co-flow partially premixed methane/air laminar flames. *Combustion and Flame*, 137:444–457, 2004.

[5] N. Peters. Laminar diffusion flamelet models in non-premixed turbulent combustion. *Progress in Energy and Combustion Science*, 10:319–339, 1984.

[6] N. Peters. Laminar flamelet concepts in turbulent combustion. In *Proceedings of the Twenty-First Symposium (International) on Combustion*, pages 1231–1250, 1986.

[7] T. Poinsot and D. Veynante. *Theoretical and Numerical Combustion*. R.T. Edwards, Inc., 2001.

[8] C.P. Chou, J.Y. Chen, C.G Yam, and K.D. Marx. Numerical modeling of NO formation in laminar Bunsen flames - A flamelet approach. *Combustion and Flame*, 114:420–435, 1998.

[9] N. Peters. *Turbulent combustion*. Cambridge University Press, 2000.

[10] P.A. Libby and F.A. Williams (ed.). *Turbulent Reacting Flows*. Academic Press, 1994.

[11] H. Pitsch and N. Peters. A Consistent Flamelet Formulation for Non-Premixed Combustion Considering Differential Diffusion Effects. *Combustion and Flame*, 114:26–40, 1998.

[12] H. Pitsch, C.M. Cha, and S. Fedotov. Flamelet modelling of non-premixed turbulent combustion with local extinction and re-ignition. *Combustion Theory and Modelling*, 7:317–332, 2003.

[13] H. Barths, N. Peters, N. Brehm, A. Mack, M. Pfitzner, and V. Smiljanovski. Simulation of pollutant formation in a gas-turbine combustor using unsteady flamelets. In *Proceedings of the Twenty-Seventh Symposium (International) on Combustion*, pages 1841–1847, 1998.

[14] K. Claramunt, R. Cònsul, D. Carbonell, and C.D. Pérez-Segarra. Laminar flamelet concept for laminar and turbulent flames, AIAA Paper 2004-796. In *Proceedings of the 42nd AIAA Aerospace Sciences Meeting and Exhibit*, 2004.

[15] H. Pitsch and H. Steiner. Large-Eddy Simulation of a turbulent piloted methane/air diffusion flame (Sandia Flame D). *Physics of Fluids*, 12(10):2541–2554, 2000.

[16] P.J. Coelho and N. Peters. Unsteady modelling of a piloted Methane/air jet flame based on the Eulerian particle flamelet model. *Combustion and Flame*, 124:444–465, 2001.

[17] P.J. Coelho and N. Peters. Numerical simulation of a Mild Combustion Burner. *Combustion and Flame*, 124:503–518, 2001.

[18] P.J. Coelho, O.J. Teerling, and D. Roekaerts. Spectral radiative effects and turbulence/radiation interaction in a non-luminous turbulent jet diffusion flame. *Combustion and Flame*, 133:75–91, 2003.

[19] S.H. Chan, X.C. Pan, and M.M.M Abou-Ellail. Flamelet Structure of Radiating CH_4-Air Flames. *Combustion and Flame*, 102:438–446, 1995.

[20] S.H. Chan, J.Q. Yin, and B.J. Shi. Structure and Extintion of Methane-Air Flamelet with Radiation and Detailed Chemical Kinetic Mechanism. *Combustion and Flame*, 112:445–456, 1998.

[21] A. Heyl and H. Bockhorn. Flamelet modeling of NO formation in laminar and turbulent diffusion flames. *Chemosphere*, 42:449–462, 2001.

[22] H. Pitsch, M. Chen, and N. Peters. Unsteady flamelet modeling of turbulent hydrogen-air diffusion flames. In *Proceedings of the Twenty-Seventh Symposium (International) on Combustion*, pages 1057–1064, 1998.

[23] J.S. Kim and F.A. Williams. Structures of flow and mixture-fraction fields for counterflow diffusion flames with small stoichiometric mixture fractions. *Journal of Computational Physics*, 53:1551–1566, 1993.

[24] A. Heyl and H. Bockhorn. Modelling of pollutant formation in complex geometries under consideration of detailed chemical mechanisms. In *Proceedings of the Fourth European Computational Fluid Dynamics Conference (ECCOMAS CFD)*, pages 808–813, 1998.

[25] H. Pitsch. Unsteady flamelet modeling of differential diffusion in turbulent jet diffusion flames. *Combustion and Flame*, 123:358–374, 2000.

[26] A.W. Cook, J.J. Riley, and G. Kosály. A laminar flamelet approach to subgrid-scale chemistry in turbulent flows. *Combustion and Flame*, 109:332–341, 1997.

[27] H. Pitsch, E. Riesmeier, and N. Peters. Unsteady flamelet modeling of Soot Formation in turbulent diffusion flames. *Combustion Science and Technology*, 158:389–406, 2000.

[28] C.S. McEnally and L.D. Pfefferle. Experimental study of nonfuel hydrocarbon concentrations in coflowing partially premixed methane/air flames. *Combustion and Flame*, 118:619–632, 1999.

[29] R. Cònsul. *Development of numerical codes for the evaluation of combustion processes. Detailed numerical simulations of laminar flames.* PhD thesis, Universitat Politècnica de Catalunya, 2002.

[30] G.P. Smith, D.M. Golden, M. Frenklach, N.W. Moriarty, B. Eiteneer, M. Goldenberg, C.T. Bowman, R.K. Hanson, S. Song, W.C. Gardiner, V.V. Lissianski, and Z. Qin. Gri-Mech 3.0, http://www.me.berkeley.edu/gri_mech/.

[31] R.J. Kee, F.M. Rupley, and J.A Miller. The Chemkin Thermodynamic Database. Technical report, Sandia National Laboratories, 1987.

[32] R.B. Bird, E.E. Stewart, and E.N. Lightfoot. *Transport phenomena*. John Wiley and Sons Inc., 1960.

[33] R.S. Barlow, A.N. Karpetis, and J.Y. Frank, J.H. Chen. Scalar profiles and NO formation in laminar opposed-flow partially premixed methane/air flames. *Combustion and Flame*, 127:2102–2118, 2001.

[34] S. Mazumder and M.F. Modest. Advanced nongray radiation model coupled with a CFD code for large-scale fire and combustion applications. Technical report, National Sciencie Foundation, 2001.

[35] W.L. Grosshandler. RADCAL: A narrow-band model for radiation calculations in a combustion environment, NIST Technical Note 1402, 1993.

[36] P.H. Gaskell and A.K.C. Lau. Curvature-compensed convective transport: SMART, a new boundedness-preserving transport algorithm. *International Journal for Numerical Methods in Fluids*, 8:617–641, 1988.

[37] S.V. Patankar. *Numerical heat transfer and fluid flow*. Hemiosphere Publishing Corporation, 1980.

[38] B.R. Hutchinson and G.D.Raithby. A multigrid method based on the additive correction strategy. *Numerical Heat Transfer, Part B*, 9:511–537, 1986.

[39] J. Cadafalch, A. Oliva, C.D. Pérez-Segarra, M. Costa, and J. Salom. Comparative study of conservative and nonconservative interpolation schemes for the domain decomposition method on laminar incompressible flows. *Numerical Heat Transfer, Part B*, 35(1):65–84, 1999.

[40] R. Cònsul, C.D. Pérez-Segarra, J. Cadafalch, M. Soria, and A. Oliva. Numerical analysis of laminar flames using the domain decomposition method. In *Proceedings of the Fourth European Computational Fluid Dynamics Conference (ECCOMAS CFD)*, volume 1.2, pages 996–1001, 1998.

[41] J. Cadafalch, C.D. Pérez-Segarra, R. Cònsul, and A. Oliva. Verification of finite volume computations on steady state fluid flow and heat transfer. *Journal of Fluids Engineering*, 124:11–21, 2002.